Model-Based Segmentation and Fusion of 3D Computed Tomography and 3D Ultrasound of the Eye for Radiotherapy Planning

M. Bach Cuadra, S. Gorthi, F.I. Karahanoglu, B. Paquier, A. Pica, H.P. Do, A. Balmer, F. Munier, and J.-Ph. Thiran

Abstract Computed Tomography (CT) represents the standard imaging modality for tumor volume delineation for radiotherapy treatment planning of retinoblastoma despite some inherent limitations. CT scan is very useful in providing information on physical density for dose calculation and morphological volumetric information but presents a low sensitivity in assessing the tumor viability. On the other hand, 3D ultrasound (US) allows a highly accurate definition of the tumor volume thanks to its high spatial resolution but it is not currently integrated in the treatment planning but used only for diagnosis and follow-up. Our ultimate goal is an automatic segmentation of gross tumor volume (GTV) in the 3D US, the segmentation of the organs at risk (OAR) in the CT and the registration of both modalities. In this paper, we present some preliminary results in this direction. We present 3D active contour-based segmentation of the eye ball and the lens in CT images; the presented approach incorporates the prior knowledge of the anatomy by using a 3D geometrical eye model. The automated segmentation results are validated by comparing with manual segmentations. Then, we present two approaches for the fusion of 3D CT and US images: (i) landmark-based transformation, and (ii) object-based transformation that makes use of eye ball contour information on CT and US images.

M. Bach Cuadra (✉), S. Gorthi, F.I. Karahanoglu, B. Paquier, and J.-Ph. Thiran
Signal Processing Laboratory (LTS5), Ecole Polytechnique Fédérale de Lausanne, Switzerland
e-mail: meritxell.bach@epfl.ch; subramanyan.gorthi@epfl.ch; isik.karahanoglu@epfl.ch; benoit.paquier@epfl.ch; jp.thiran@epfl.ch

A. Pica
Radiation Oncology Department, Lausanne University Hospital (CHUV), Switzerland
e-mail: alessia.pica@chuv.ch

H.P. Do
Institute of Applied Radiophysics, Lausanne, Switzerland
e-mail: dohuuphuoc@hotmail.fr

A. Balmer and F. Munier
Ophthalmic Hospital Jules Gonin, Lausanne, Switzerland
e-mail: aubain.balmer@fa2.ch; Francis.Munier@fa2.ch

J.M.R.S. Tavares and R.M.N. Jorge (eds.), *Computational Vision and Medical Image Processing: Recent Trends*, Computational Methods in Applied Sciences 19,
DOI 10.1007/978-94-007-0011-6_14,

Keywords Parametric Active Contours · Model-based segmentation · Multi-model image fusion · Ultrasound imaging · Computer tomography · Eye imaging · radiotherapy

1 Introduction

Retinoblastomas are one of the common primary ocular malignancies in childhood. They are very aggressive tumors appearing before the age of four years old, hereditary in 40% of the cases, and they account for 5% of childhood blindness [8]. Linear accelerator (LINAC) based conformal stereotactic radiotherapy (SRT) is one of the most precise radiotherapy treatments for retinoblastomas[1] to control advanced, often chemotherapy resistant, intra-ocular tumors in progression after chemotherapy and focal ophthalmologic therapies in children. Thus, primary endpoint of such radiation therapy is the eye and visual function preservation following intra-ocular progression. Therefore, delineating the tumor in order to optimize radiation doses, allowing minimization of dose to adjacent developing tissues is a crucial goal. To this end, patients usually undergo a multi-modal imaging: First, Computed Tomography (CT) scan, which is very useful in providing information on physical density for dose calculation and morphological volumetric information, and second, ophthalmologic examination with 2D and 3D ultrasound (US) and fundus pictures, which allow a very accurate definition of the tumor volume thanks to its high spatial resolution. Actually, thanks to its improving quality, the use of US imaging is increasing in ophthalmology [9,19]. Note that such multi-modal CT-US imaging framework has been already suggested for the therapy of other organs like the liver and kidney [15, 18] but, as far as we know, this is the first attempt of combining these two modalities in the radiotherapy planning of the eye.

In the current therapy planning, 2D and 3D ultrasound imaging and fundus photographs are qualitatively used for diagnosis, gross tumor volume definition and follow-up but they are not integrated in the treatment planning. Notice that tumor is not always visible un CT images and thus the use of ultrasound or fundus photographs is crucial. Our ultimate goal is the fusion of 3D US imaging, optimal for tumor volume delineation, and CT imaging, optimal for dose calculation and treatment planning. Through an automated segmentation of gross tumor volume (GTV) in the 3D US along with the registration to the CT, the rather inaccurate and time-consuming manual volume definition[2] could be shortened and the volume definition would become highly reproducible and comparable, overcoming the intrinsic problems of inter- and intra-user variability, thus making radiation treatment techniques amenable to standardization.

[1] This treatment has been developed at the Lausanne University Hospital (CHUV) in collaboration with the Jules Gonin University Eye Hospital. It reduces the risk of long term complications in external beam radiation therapy [12].

[2] By manual volume definition we mean the manual segmentation of organs at risk and tumor, when possible, in the CT that defines the treatment planning. However, in some cases, the gross tumor volume cannot be manually segmented since it is not visible.

The overall framework is represented in Fig. 1: Input images are represented on the left side, the methodology is described inside the dashed box and the resulting treatment planning, including the tumor, is shown as output on the right hand side. The methodology goes from top to bottom and from left to right: first, eye segmentation is done in the CT, second, through image registration we can find the eyeball area and lens in the US and then, we will proceed to the tumor segmentation in the US. Finally tumor-segmentation in US is transferred to the radiotherapy planning on the CT through the image fusion.

In this paper we present the first steps towards this multi-modal imaging framework for the radiotherapy planning of the eye. We present an automated segmentation of the eye exploiting the prior knowledge that we have on eye's anatomy; the prior knowledge about the eye is incorporated by parameterizing the active contour with a 3D geometrical model. Then, we will present the fusion of these two modalities using landmark-based and object-based transformations. This work is an extended version of our previous work in [1]. The paper is organized as follows. In Sect. 2, a brief state-of-the-art on eye segmentation techniques will be presented, focusing on the ones that exploit a geometrical eye model. In Sect. 3, the parametric Active Contour segmentation of the eye ball and lens in the CT image will be shown. Results from the automated segmentation will be compared with manual segmentations done by an expert. In Sect. 4, we will use landmark-based and object-based rigid registration to initially fusion the CT and 3D US images along with qualitatively results. Finally, discussion and future works will be summarized in Sect. 5.

2 Related Works on Eye Segmentation

Related works on segmentation of organs of sight are very sparse in time as well as in methodology (see Table 1). Souza et al. [17] segmented the extraocular muscles in CT images with mathematical morphology; D'Haese et al. [6] segmented the eyeball, lens and optic nerve by atlas-based registration in MR images; Cates et al. [5] segmented the eyeball and optic nerve on Visible Human Female data using

Table 1 Summary of related works on segmentation of organs of sight

Works	Image modality	Segmentation target	Segmentation method	Eye model
Bondiau (1997), [3]	CT, Fundus	Hough transform	Sclera, lens, optic nerve, clips	Yes
Souza (2000), [17]	CT	Mathematical morphology	Extra ocular muscles	No
Dobler (2002), [7]	CT, MR, Fundus	–	Tumor and complete eye anatomy	Yes
D'Haese (2003), [6]	MR	Atlas-based registration	Sclera, lens, optic nerve, chiasm	Yes
Cates (2005), [5]	VHF	Watershed	Eyeball, optic nerve	No
Bekes (2008), [2]	CT	Soft classification	Sclera, lens, optic nerve, chiasm	Yes

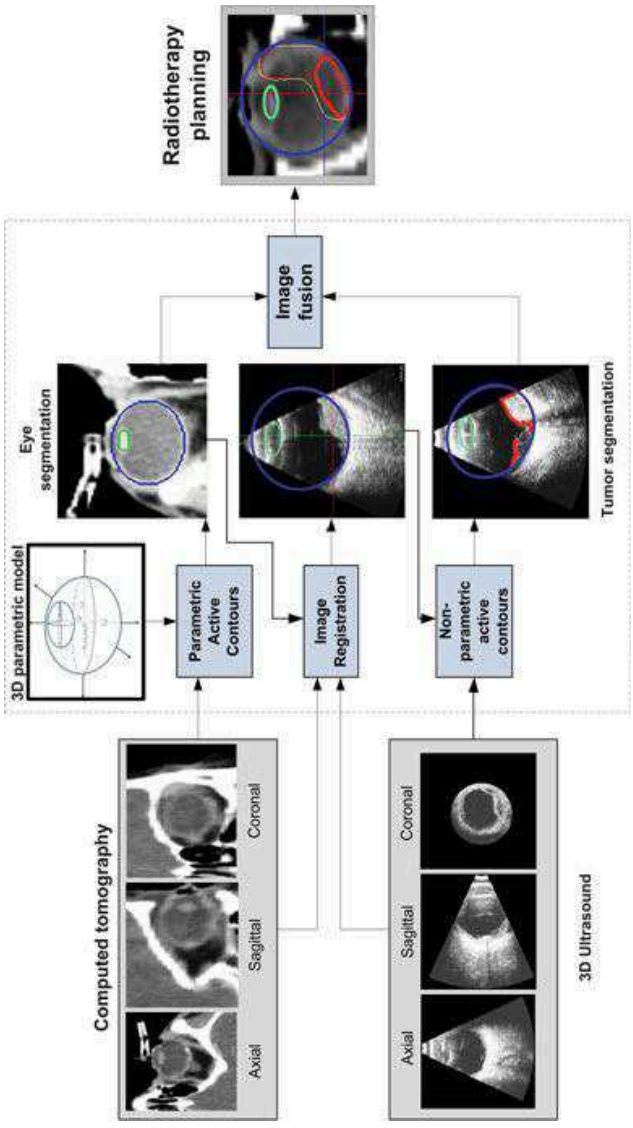

Fig. 1 Global framework for model-based segmentation and image fusion of 3D CT and 3D ultrasound of the eye for radiotherapy planning. Input images are represented on the left side, with axial, coronal and sagittal views of each. Methodology is described inside the dashed box. From *top-bottom* and *left-right*: First, eye segmentation is done in the CT, using the parameterized active contours; second, through image registration we can find the eyeball area and lens in the US; third, we will proceed to the tumor segmentation. By fusion, tumor will be superposed to the treatment planning in the CT

watershed method. Other works have explicitly taken into account the particular geometrical shape of the eye. The use of a geometrical eye model was suggested very early by Bondiau et al. [3] in 1997. Their goal was the eye reconstruction to improve protontherapy treatment of ocular tumors. Their approach consisted in building an eye model (sclera, lens, optic nerve and tantalum clips) and adapting each structure of the model to the CT image through a Hough transform. They also presented preliminary results of the fusion of CT with retinographies. Later, Dobler and Bendl [7] presented a very precise 3D geometric and hierarchical model of the eye composed in total of nine structures (sclera, vitreous body, cornea, anterior chamber, lens, iris, macula, optical nerve, and optical disc) with each structure described either by an ellipsoid or an elliptic cylinder. Their goal was to combine the 3D geometrical eye model along with the 3D CT, the 3D MR and the 2D fundus diagram for a new proton therapy system planning called *OCTOPUS* [13]. The setting of the model parameters was done by manual measurements on ultrasound images. Then, the model was adapted to the CT and MR images by registration[3] and 3D to 2D projections were used to adapt the model to the fundus photographs. Recently, in Bekes et al. [2] introduced a simplified eye model consisting in sclera (modeled as a sphere), the lens (modeled as an ellipsoid), the optic nerve and chiasm (cylinder). In their approach the selection of parameters was almost completely automated to minimize user interaction. Their model-based segmentation was performed on CT images based on thresholding and soft classification methods.

As in [2, 3, 7], our method makes use of a 3D geometrical eye model. Our main contribution regarding the existing approaches is the use of parameterized active contours (AC) to represent the eye. This will allow us to take advantage of this mathematically well-formulated framework and exploit the edge and region characteristics from the CT scan to adapt the model for every patient. Unlike [2, 3], we will represent the eye structures by ellipsoids. We are currently interested in the segmentation of eye ball and lens only, but other structures can be easily included in such framework either by parametric or non-parametric active contours. The idea of a multi modal framework for improving therapy planning [3, 7] is not new neither. However, as far as we know, our work is the first one that attempts in combining 3D ultrasound and CT scans.

3 Eye Segmentation in the Active Contour Framework

The CT image properties and the very well known geometry of the eye lead to an adaptation of the active contours theory [4] which aims at finding a curve C that minimizes the energy functional E, designed to be minimal when C has found the desired contour. The general expression of E is given by

$$E(C) = E_{image}(C) + E_{smooth}(C), \tag{1}$$

[3] The type of registration process used in [7] for adapting the model to the 3D images was not explicitly mentioned in that paper.

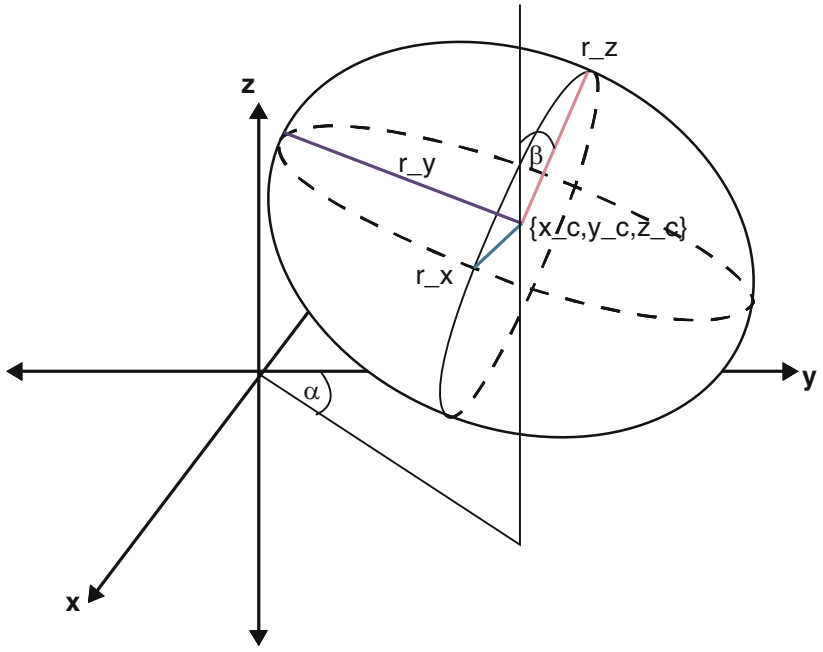

Fig. 2 The proposed 3D parametric model of the eye consisting of ellipsoids for the eye ball and the lens. The model parameters for the eye lens are $\theta_{lens} = \{x_c, y_c, z_c, r_x, r_y, r_z, \alpha, \beta\}$ corresponding to the center coordinates, the length of the axes and the rotation angles. Model parameters for the eye ball are $\theta_{ball} = \{x_c, y_c, z_c, r_x, r_y, r_z\}$ thus α and β angles are neglected since these values are going to be varying around 0

Here, we take advantage of using a parameterized model, which means that the analytical expression of C is known everywhere on the domain of the image and is defined by a set of parameters θ. Thus, C is a parameterized model based on the ellipsoid parameters $\theta = \{x_c, y_c, z_c, r_x, r_y, r_z, \alpha, \beta\}$ corresponding to the center coordinates, the length of the axes and the rotation angles (see Fig. 2).

Obviously, we will not impose any E_{smooth} term since our parameterized curve is already smooth. Then, the E_{image} term can be expressed in two sub-terms:

$$E_{image}(C(\theta)) = E_{boundary}(C) + E_{region}(C), \tag{2}$$

which are computed from the image features.

$E_{boundary}$ attracts the curve towards the object boundaries using an edge detecting function f, and in this work is given by:

$$E_{boundary} = \int_C f(C, s)ds. \tag{3}$$

Such edge detection function works fine in CT images but other gradient-based functions should be used for other images. Once applied to the image I, $f(C, s)$ has to return an optimum value (minimum in our case) when its variables, which are the curve spatial coordinates $(x(\theta, s), y(\theta, s), z(\theta, s))$ mapped by the model on the image, are matching the edges of the object to be delineated. Therefore, f can be of the form:

$$f(C,s) = \begin{cases} -(I_{eq}(C,s) * G_\sigma) & \text{if } I_{eq}(C,s) > T_h, \\ 0 \text{ otherwise.} \end{cases} \tag{4}$$

where T_h is a threshold applied on the equalized image intensity and empirically set to 0.8, G is the Gaussian function with standard deviation σ and $I_{eq} * G_\sigma$ represents the smoothed version of the equalized image histogram I.

E_{region} captures the regional statistics to drive C towards homogeneous regions. The idea here is to maximize the difference between two statistical descriptors (the mean value of intensities) related to two regions of the image, Ω_{in} and Ω_{out}, in our case, respectively the inside and the outside of an ellipsoid within a selected region of interest around the lens. Formally

$$E_{region} = -|\text{mean}(\Omega_{in}) - \text{mean}(\Omega_{out})|. \tag{5}$$

The segmentation problem is now reduced to an energy optimization problem. Thus, the parameter-set θ that results in minimum energy provides the segmentation of the objects of interest.

$$\theta_{\text{object}} = \arg\min_{\theta} E(C(\theta)). \tag{6}$$

From our experiments, we found that boundary-based term ($E_{boundary}$) alone is sufficient for the accurate segmentation of the eye ball. Similarly for the lens, we found that region-based term (E_{region}) alone is sufficient. Hence, for the results that we present in the Sect. 3.2, we use only $E_{boundary}$ term for the eye ball, and only E_{region} term for the lens segmentation.

3.1 Practical Implementation and Optimization Strategy

3.1.1 Eyeball Segmentation

We observed from our experiments that rotation angles for the eye ball are always varying around 0 (this particularly linked to the CT image acquisition protocol used here). Hence, we simplified the eye ball segmentation by neglecting these angles: $\{\alpha, \beta\}$. As a result, the number of parameters to be optimized for the eye ball are 6. We do not apply the optimization directly to the CT scan but to an *edge detected image* (see Fig. 3a). This image is obtained as defined previously in (4): First, histogram is equalized to expand intensity values and enhance sharp edges; second, a threshold of 0.8 is applied to extract the eyeball contours; third, we smooth by a Gaussian filter.

3.1.2 Lens Segmentation

As mentioned previously, we will use region information to segment the lens. Using the edge information similar to the eyeball is not preferred since lens boundary

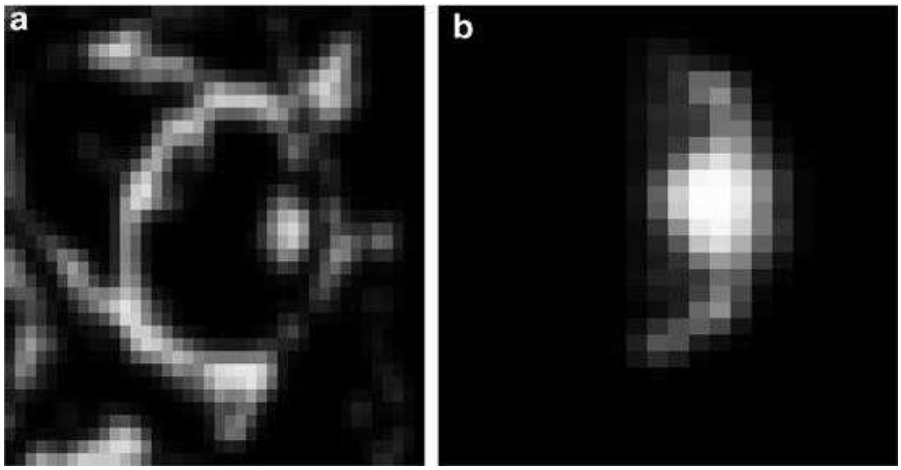

Fig. 3 Input images for the eyeball (**a**) and lens (**b**) segmentation for one of the patients

is located near the eyeball edge. Here, eight parameters defining the ellipsoid will be used. We will proceed in a small region of interest corresponding to the upper part of the eyeball where the lens is located (see Fig. 3b). This is done to obtain a comparable volume inside and outside the lens and ensure the good behavior of the regional energy term.

3.1.3 Optimization

The optimization is implemented with a Nelder-Mead simplex search included in the Matlab *fminsearch* function. Note that a set of parameters such as θ includes elements of different nature and therefore their range is very different. For example a semi-axis of the eye ball ranges from 5 to 20 mm while an angle ranges from 1 to 360 degrees. To overcome this problem we proceed to the optimization iteratively using three subsets of parameters, $[x_c, y_c, z_c]$, $[r_x, r_y, r_z]$, and $[\alpha, \beta]$ (actually only the first two subsets for the eye ball). Moreover the algorithm is applied twice per object (first expanding the ellipsoid and later shrinking it). Histogram equalization of the image is performed as a pre-processing step. Eye ball optimization is initialized by user clicks, (center coordinates x_c, y_c, z_c and the radius in z direction, r_z). Lens optimization is restricted to one half of the eyeball only. The overall optimization algorithm is summarized as follows:

1. **Input data**
   Image with smoothed edges (lens) or threshold image (eyeball) (see Fig. 3)
2. **Ellipsoid initialization**
   Smaller (eyeball)/Bigger (lens)

3. **Iterative loop**
   Three iterations loop optimizing two subsets of parameters for the eyeball, three subsets for the lens
4. **Security check**
   To avoid too much deviation from solution (axes length can be neither longer nor shorter than usual eye size)
5. **Stopping conditions**
   After $N = 15$ iterations or if the ellipsoid is outside normal anatomy size
6. **Go back** to 2
   Bigger than eyeball/lens, now ellipsoid shrinks instead of growing

3.2 Segmentation Results and Validation

Segmentation results for three patients are presented in this section. Fore each patient, only the eye under radiotherapy planning is considered. CT images are acquired in the Lausanne University Hospital, on a LightSpeed VCT General Electric Medical Imaging scanner. Images have a resolution of $0.7 \times 0.7 \times 2\,\text{mm}^3$ and volume of interest around the eye area is of $90 \times 90 \times 30$ voxels. Results are shown in Fig. 4. By visual inspection on axial and sagittal views we can conclude that the segmentation is good for both lens and eyeball. 3D view reconstruction is also shown, note that the segmentation of the skull has been done simply by threshold for visualization purposes. Fitted ellipsoid parameters (the radii for both eyeball and lens and the rotational angles of the lens) are shown Table 2. Quantitative evaluation is done by comparison with manual segmentations done by an expert. We used the Dice Similarity Measure (DSM) as relative index of similarity between manual (m) and automated (a) segmentations. DSM is defined as

$$DSM^{o}_{a,m} = \frac{2 \cdot N_{a \cap m}}{N_a + N_m}, \tag{7}$$

where N_a and N_m are the voxels belonging to the object (ball and lens) o according to the automated and manual segmentation methods a and m, respectively, and $N_{a \cap m}$ is the number of voxels belonging to the object according to both methods. Although $DSM > 0.7$ is considered as an excellent agreement between the two segmentations, DSM is hardly interpreted as an absolute value but as a value to compare the similarities between pairs of methods. Resulting DSM values are shown in Table 3 presenting a very high agreement between the manual and the automated segmentation for the eyeball and the lens.

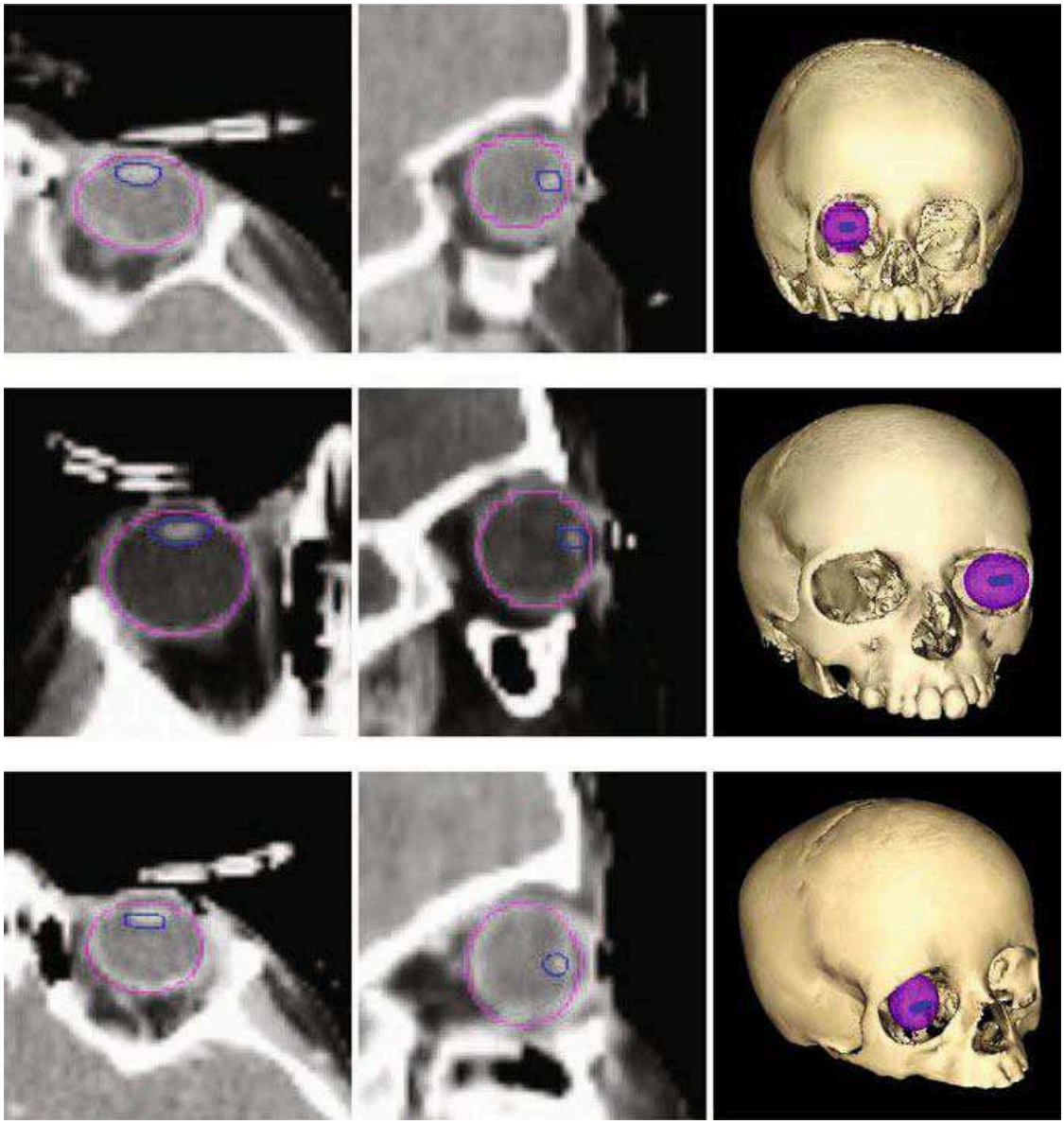

Fig. 4 Axial, sagittal and 3D views of the automated segmentation results of the eye ball and the lens, for three patients

Table 2 Computed radii and rotational angles for the eye ball and the lens, obtained from the automated CT image segmentation

	Eye ball	Lens	
	(r_x, r_y, r_z) in mm	(r_x, r_y, r_z) in mm	(α, β) in degrees
Patient 1	(10.0, 9.1, 10.0)	(3.6, 1.8, 2.0)	(186.6, 165.4)
Patient 2	(12.3, 10.6, 12.6)	(3.1, 1.5, 1.5)	(181.7, 181.1)
Patient 3	(10.5, 9.8, 11.0)	(4.9, 2.2, 2.4)	(185.3, 177.0)

Table 3 Quantitative evaluation for the eyeball and the lens

	Volume (mm^3)			
	Manual	Automated	Error	DSM
Eyeball				
Patient 1	4764	4827	1.33%	89.9%
Patient 2	7758	7798	0.52%	92.6%
Patient 3	6114	5543	9.33%	90.2%
Lens				
Patient 1	141	102	−27.7%	78.4%
Patient 2	205	215	4.9%	76.9%
Patient 3	217	219	0.9%	76.8%

4 Image Fusion

As introduced earlier, one of our goals is the fusion of CT and 3D ultrasound images. Other approaches in the literature have already suggested the fusion of multi-modal images such as CT and fundus photographs [3, 7] to improve the treatment planning precision, specifically to better define the gross tumor volume in the CT space. To proceed to this fusion, they computed the flattening geometrical distortion from 3D (the CT scan) to 2D (the fundus photograph) spaces. However, the nature of our problem is slightly different. In our case, we do have two 3D volumes to match, thus we have a volume-to-volume registration problem.

The ophthalmic 3D ultrasound images used here are acquired with OTI Ophthalmic Technologies Inc. [14]. The OTI-Scan 3D is one of the most advanced ophthalmic ultrasound system available today. The internal rotator assembly generates a 3D image in less than 2 s with a 0.1 mm resolution in each X, Y, and Z direction. An example of such acquisition is shown in Fig. 1.

Multi-modal volume registration is a widely studied problem in medical imaging [10]. There exists however few studies related to the 3D ultrasound registration with any other modality [15, 16, 18] and none of them is dedicated to the eye. Multi-modal registration is often applied on image volumes coming from the same subject. Its registration aims at compensating for difference in positions of the patient during the image acquisition process of both modalities. Thus, a rigid registration (three translations and three rotations) is often enough to this end. Often, prior to voxel-based registration, a global supervised initialization is computed to ensure a better convergence of any further registration. This is particularly needed in our case since CT and US images are acquired with very different fields of view. Note that while the CT contains the whole head, the US image only presents partially one eye.

In this section we present two *supervised* registration approaches for an initial fusion of CT and US. By *supervised* we mean that both methods needs user interaction.

4.1 Landmark-Based Registration

We choose a landmark based transformation with six parameters (three rotations and three translations) that will give the best fit mapping between corresponding point sets of the moving (US) and the target (CT) images, in a least squares sense. Landmarks selection, particularly in US image, is not an easy task and must be done by an expert. Landmark selection and registration has been done with the MITK application [11].

Three landmarks per patient and image have been selected. It is not always possible to select the same landmarks between patients. If the tumor is visible in the CT (this is not the case for Patient 2) it becomes a good landmark since its localization is easy in both modalities. The head of the optic nerve is a good landmark as well but it can be sometimes behind a tumor and thus not clearly visible in the US where a shadow behind the tumor mass appear (as it occurs for Patient 1). The summary of selected landmarks for each patient is shown in Table 4.

At this point we can proceed to the fitting of the rigid parameters that best approximate these three locations. Resulting transformation parameters (rotational angles in degrees and translations in mm) are shown in Table 5. Visualization of resulting registration is done by superposing transformed US image and moving landmarks (M1, M2 and M3) onto the CT and are shown in Fig. 5. Eyeball contour and lens have been superposed as well. Visual inspection shows a good initialization but it is difficult to quantify the accuracy of this registration. The root mean square error

Table 4 Summary of selected landmarks for each patient and Root Mean Square Error (RMSE) before (*top row*) and after (*bottom row*) registration

	Landmark 1	Landmark 2	Landmark 3	RMSE
Patient 1	Lens	Tumor 1	Tumor 2	16.32
				0.95
Patient 2	Optic nerve	Lens	Eye center	23.30
				0.36
Patient 3	Optic nerve	Lens	Tumor	16.27
				1.36

Table 5 Rigid transformation parameters estimated by the landmark-based registration. X, Y, Z are the axis directions, rotation angles are in degrees and translations are in mm

		X	Y	Z
Patient 1	*Rotation*	46.94	−60	161.32
	Translation	11.51	−57.19	24.10
Patient 2	*Rotation*	5.41	89.56	−84.95
	Translation	40.82	−12.36	51.58
Patient 3	*Rotation*	−3.49	−32.31	3.46
	Translation	−80.00	−144.11	179.37

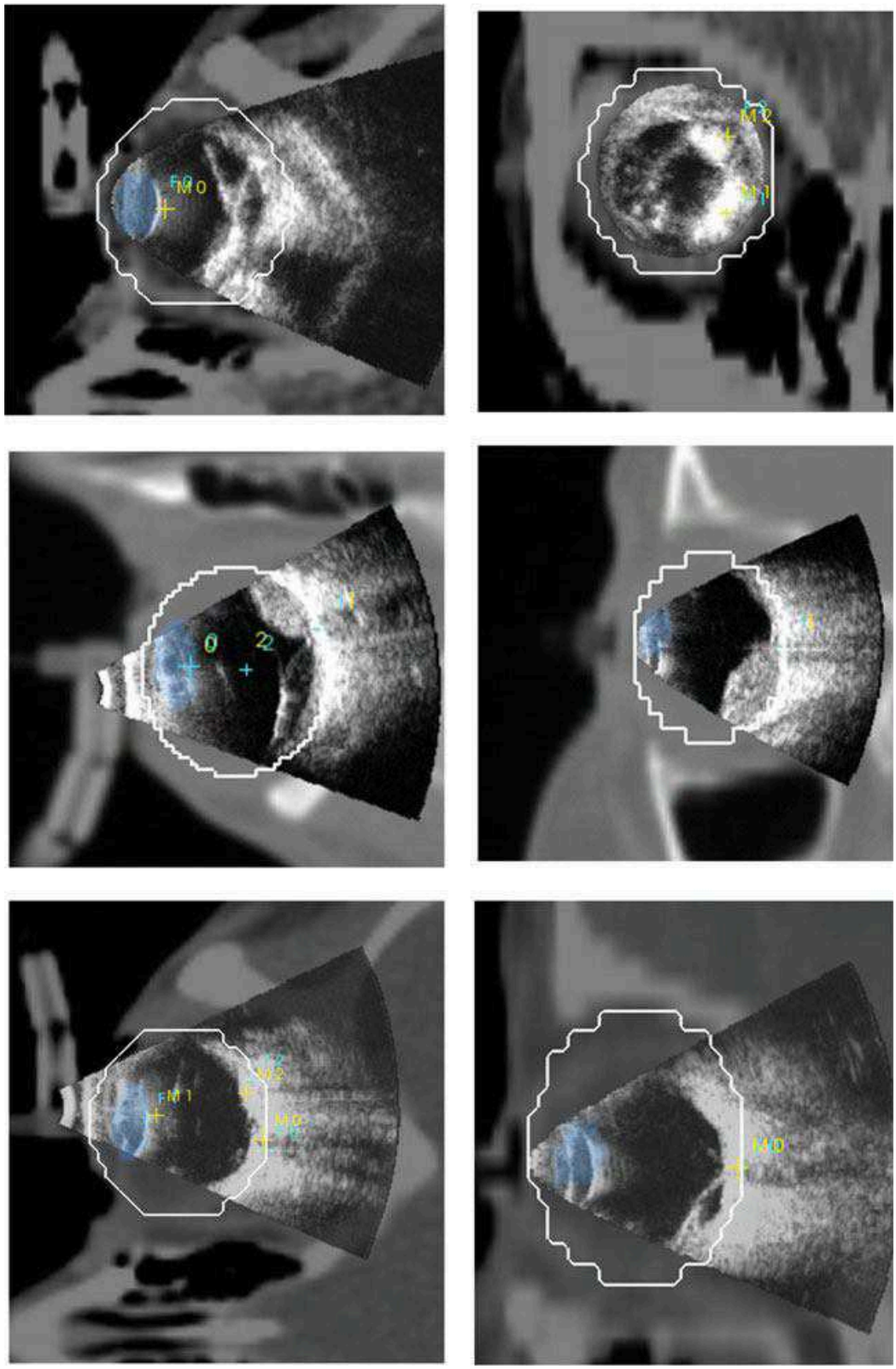

Fig. 5 Landmark-based registration results for three patients. Ultrasound is superposed to the CT image. Moving landmarks are in yellow, fixed landmarks are in cyan. The lens mask in blue and the eyeball contour in black. (**Top row**) Patient 1: Axial (*left*) and coronal (*right*) views of superposition. Landmarks are in the back of the lens (0), and in tumors (1 and 2). (**Middle row**) Patient 2: Axial (*left*) and sagittal (*right*) views of superposition. Landmarks are in the back of the lens (0), head of the optic nerve (1) and center of the eye ball (2). (**Bottom row**) Patient 3: Axial (*left*) and sagittal (*right*) views of superposition. Landmarks are in the head of the optic nerve (0), back of the lens (1) and small calcified tumor (2)

(RMSE) between moving and target landmarks before and after the transformation is shown in Table 4. This gives us an idea only about the accuracy in fitting the selected landmarks but about not the quality of the transformation.

The main problem that we have faced with the current landmark-based approach is that identification of anatomical corresponding landmarks on CT and US images is a tedious and time consuming task. For example, it took around 30 min per patient for an expert ophthalmologist to select the landmarks. Thus, landmark-based registration will always need the intervention of an expert for identifying corresponding point sets. In order to avoid these inconveniences, we propose in the next Section another type of initialization, an *object-based registration*.

4.2 Object-Based Transformation

As mentioned previously, initial images have different acquisition orientation. Thus, first step in the object-based registration is to change US orientation to CT. This is done by simply rotating the image accordingly. Still both images are not precisely in the same space as shown in Fig. 6 (left panel). We apply a second transformation by roughly selecting the eyeball center in both images and then fitting them by a translation. The result of this initialization is shown in Fig. 6 (right panel). Then, we create from the segmented eyeball and lens (CT) a mesh that will now represent the target object to match. These points are represented in Fig. 7 (left panel). Then, even a non expert user proceed to select few points (around 25) corresponding to

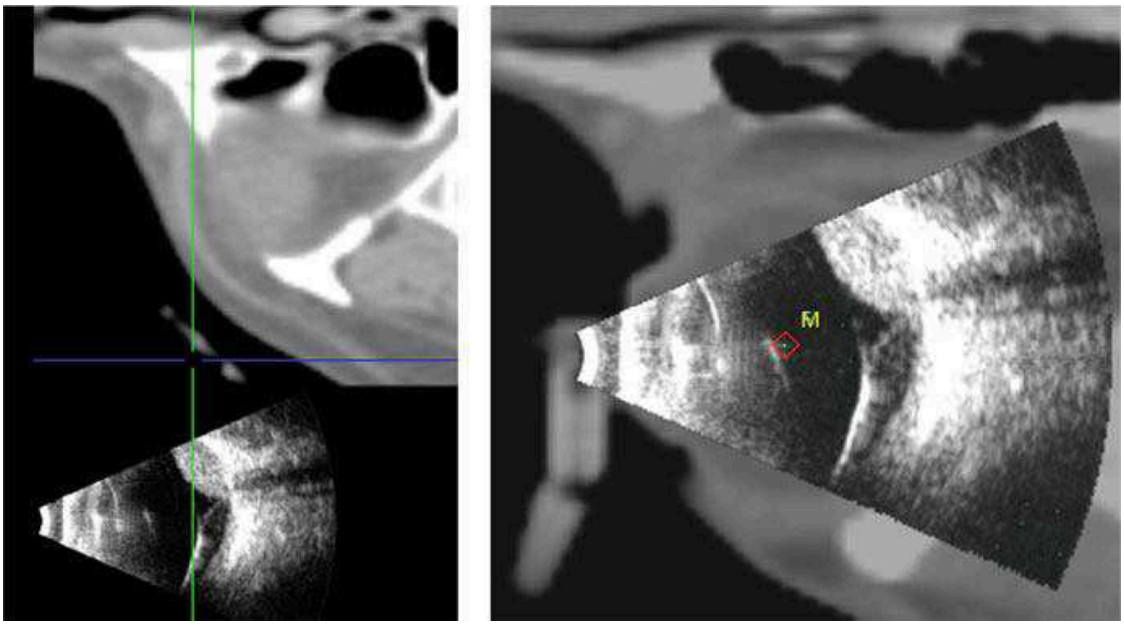

Fig. 6 Object-based initialization: *left* panel is the original position of both modalities after changing acquisition orientation of US image; *right* panel is the result of the rigid transform computed from eyeball center landmarks

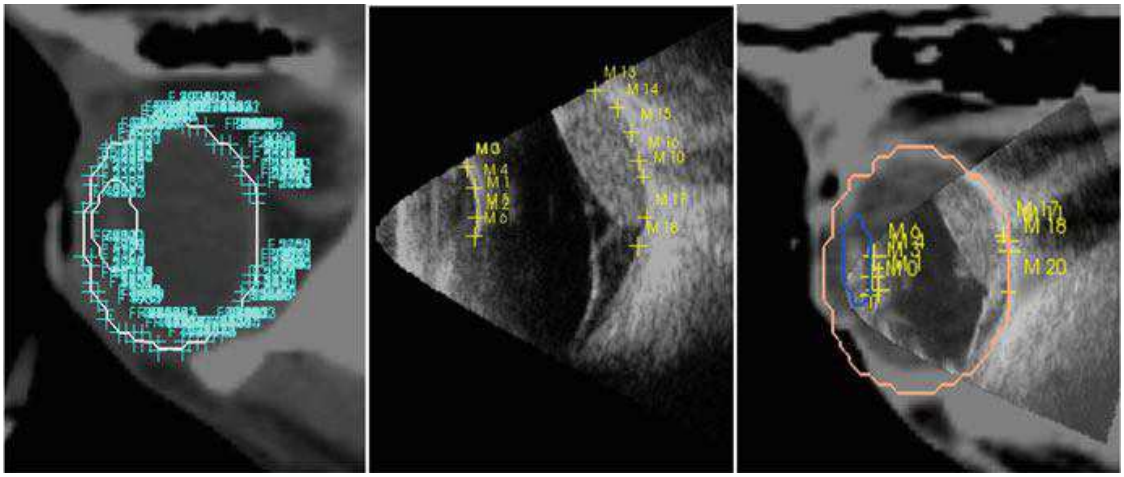

Fig. 7 Object-based registration: *left* panel are the mesh points of the eyeball and lens in the CT space; *middle* panel are the selected points on the US corresponding to the back of the lens and the back of the eye; *right* panel is the final positioning after ICP rigid registration

the back edges of the eyeball in the US, as well as some points in the back border of the lens. An example of such points are shown in Fig. 7 (middle panel)[4]. The whole procedure takes only few minutes. Finally, ICP algorithm is applied to compute the rigid transformation between these two sets of points. The resulting registration is shown in Fig. 7 (right panel).

At this point we cannot conclude whether landmark-based or object-based registration is better since we do not have a gold standard to compare with. Moreover, the object-based registration presented here is rather preliminary: mesh creation should be improved and more patients should be tested. Qualitatively, results of both transformations are very similar and we consider both initializations as good for a further voxel-based volume registration. However, object-based registration is performed in 2 or 3 min by even a non-expert user while landmark-based registration takes around 30 min and needs from an expert.

5 Discussion

In this paper, we have presented our preliminary work towards a multi-modal framework for the radiotherapy planning of retinoblastomas. To our knowledge, this is the first attempt to combine 3D CT and 3D US for the eye radiotherapy. In the present work we have presented a model-based segmentation of the eye ball and the lens on the CT images. The main difference compared to the existing model-based segmentation methods is that here we proceed by using the well formulated

[4] Every point is represented by a cross and tags enumerating it. However since for this mesh we have a lot of points the tags appear all superposed and make the visualization a little strange.

active contour framework. Evaluation in comparison with manual segmentation has shown a good accuracy of our segmentation model. Moreover, we have also computed a first required initialization of the rigid transformation that brings the CT, and thus the eye model, and the US into the same space. Two procedures have been suggested for the initial alignment: landmark-based and object-based registration. Landmark-based registration requires an expert user interaction for selecting the landmarks and this takes a considerable amount of time. The suggested object-based approach overcome this problem and resulting registration seems very close to the landmark-based one. Further research will be on creating a ground truth for registration assessment. For instance by creating simulated US data from CT or being able to scan an eye *phantom*. Also, as in [7], other registration strategies could be considered as fitting the eye model directly to US and then, trough the model, compute the transformation between both images. As well, we believe that the optic nerve should be included in the model. Finally, tumor segmentation on the US image should be investigated.

Acknowledgements This work is supported by the Centre d´Imagerie BioMédicale (CIBM) of the University of Lausanne (UNIL), the Swiss Federal Institute of Technology Lausanne (EPFL), the University of Geneva (UniGe), the Centre Hospitalier Universitaire Vaudois (CHUV), the Hôpitaux Universitaires de Genève (HUG) and the Leenaards and the Jeantet Foundations.

References

1. Bach Cuadra, M., Gorthi, S., Karahanoglu, F.I., Salvador, F., Pica, A., Do, H., Balmer, A., Munier, F., Thiran, J.P.: Model-based segmentation and image fusion of 3D computed tomography and 3D ultrasound of the eye for radiotherapy planning. In: Second ECCOMAS Thematic Conference on Computational Vision and Medical Image Processing, pp. 53–58 (2009)
2. Bekes, G., Máté, E., Nyúl, L.G., Kuba, A., Fidrich, M.: Geometrical model-based segmentation of the organs of sight on CT images. Med. Phys. **35**, 735–743 (2008)
3. Bondiau, P.Y., Malandain, G.: Eye reconstruction and CT-retinography fusion for proton treatment planning of ocular diseases. In: CVRMed-MRCAS'97, *LNCS*, vol. 1205, pp. 705–714. Springer (1997)
4. Caselles, V., Kimmel, R., Sapiro, G.: Geodesic active contours. Int. J. Comput. Vis. **22**(1), 61–79 (1997)
5. Cates, J.E., Whitaker, R.T., Jones, G.M.: Case study: an evaluation of user-assisted hierarchical watershed segmentation. Med. Image Anal. **9**(6), 566–578 (2005)
6. DHaese, P., Duay, V., Li, R., du Bois dAische, A., Merchant, T., Cmelak, A., Donnelly, E., Niermann, K., Macq, B., Dawant, B.: Automatic segmentation of brain structures for radiation therapy planning. In: Medical Imaging: Image Processing, ISCAS. SPIE (2003)
7. Dobler, B., Bendl, R.: Precise modelling of the eye for proton therapy of intra-ocular tumours. Phys. Med. Biol. **47**(4), 593–613 (2002)
8. Donaldson, S., Smith, L.: Retinoblastoma: biology, presentation, and current management. Oncology **3**(10), 45–51 (1989)
9. Fenster, A., Downey, D., Cardinal, H.: Three-dimensional ultrasound imaging. Phys. Med. Biol. **46**(5), 67–99 (2001)
10. Maintz, J., Viergever, M.A.: A survey of medical image registration. Med. Image Anal. **2**(1), 1–36 (1998)
11. Maleike, D., Nolden, M., Meinzer, H.P., Wolf, I.: Interactive segmentation framework of the medical imaging interaction toolkit. Comput. Meth. Programs Biomed. **96**(1), 72–83 (2009)

12. Munier, F., Verwey, J., Pica, A., Balmer, A., Zografos, L., Abouzeid, H., Timmerman, B., Goitein, G., Moeckli, R.: New developments in external beam radiotherapy for retinoblastoma: from lens to normal tissue-sparing techniques. Clin. Exp. Ophthalmol. **36**(1), 78–89 (2008)
13. OCular TumOur Planning UtilitieS (OCTOPUS). http://www.dkfz.de/en/medphys/therapy_planning_development/projects/octopus.html
14. Ophthalmic Technologies Inc. (OTI), Canada. http://www.opko.com/
15. Penney, G., Blackall, J., Hamady, M., Sabharwal, T., Adam, A., Hawkes, D.: Registration of freehand 3D ultrasound and magnetic resonance liver images. Med. Image Anal. **8**, 81–91 (2004)
16. Roche, A., Pennec, X.M.G.A.N.: Rigid registration of 3-D ultrasound with MR images: a new approach combining intensity and gradient information. IEEE Tran. Med. Imag. **20**(10), 1038–1049 (2001)
17. Souza, A., Ruiz, E.: Fast and accurate detection of extraocular muscle borders using mathematical morphology. In: Engineering in Medicine and Biology Society, 2000. Proceedings of the 22nd Annual International Conference of the IEEE, vol. 3, pp. 1779–1782 (2000)
18. Wein, W., Brunke, S., Khamene, A., Callstrom, M., Navab, N.: Automatic CT-ultrasound registration for diagnostic imaging and image-guided intervention. Med. Image Anal. **12**, 577–585 (2008)
19. Yannuzzi, L.A., Ober, M.D., Slakter, J.S., Spaide, R.F., Fisher, Y.L., Flower, R.W., Rosen, R.: Ophthalmic fundus imaging: today and beyond. Am. J. Ophthalmol. **137**(3), 511–524 (2004)